JOURNAL OF GEOPHYSICAL RESEARCH, VOL. 111, D23210, doi:10.1029/2006JD007279, 2006



# Measurements of atmospheric parameters during Indian Space Research Organization Geosphere Biosphere Program Land Campaign II at a typical location in the Ganga Basin: 2. Chemical properties

Vinod Tare,[1] S. N. Tripathi,[1] N. Chinnam,[1] A. K. Srivastava,[1] Sagnik Dey,[1] M. Manar,[1] Vijay P. Kanawade,[1] A. Agarwal,[1] S. Kishore,[1] R. B. Lal,[1] and M. Sharma[1]

Received 9 March 2006; revised 9 July 2006; accepted 10 August 2006; published 14 December 2006.

[1] This paper attempts to analyze the chemical compositions of the near surface aerosols at a typical location in the Ganga basin with an emphasis on delineating the source of aerosols in foggy/hazy conditions. Collocated measurements of a number of atmospheric and aerosol parameters along with simultaneous sampling of near surface aerosols of size less than 10 $\mu$m ($PM_{10}$) were made as part of an intense field campaign launched under the Indian Space Research Organization Geosphere Biosphere Program (ISRO-GBP) in December 2004. $PM_{10}$ and black carbon (BC) mass concentration was found to be significantly higher during the foggy/hazy period. Much of the $PM_{10}$ mass ($\sim$81%) was due to fine/accumulation mode particles (0.1–0.95 $\mu$m). Significant proportions of water soluble ions such as $NH_4^+$, $K^+$, $Na^+$, $Cl^-$, $NO_3^-$ and $SO_4^{2-}$ were present in the fine mode particles while considerable amounts of $Ca^{2+}$ and $Mg^{2+}$ along with $NH_4^+$, $K^+$, $Na^+$, $Cl^-$, $NO_3^-$ and $SO_4^{2-}$ were found in the coarse mode particles. Also, water soluble ions $NH_4^+$ and $NO_3^-$ were significantly higher; however, $Na^+$, $K^+$, $SO_4^{2-}$ and $Cl^-$ did not show significant difference between foggy/hazy and clear days. In contrast, $Ca^{2+}$, $Mg^{2+}$ and acid soluble metals were significantly lower during foggy/hazy days as compared to the clear days. Presence of higher amounts of $NH_4^+$, $K^+$, $NO_3^-$ and $SO_4^{2-}$ associated with very low values (<5 ppmv) of $SO_2$ despite considerable plausible emissions due to fossil fuel and biomass burning in the region suggests that loading of fine mode aerosols in the region could have been enhanced through reactions of gaseous pollutants on the solid surfaces. These results along with the findings presented in the companion paper indicate that prolonged foggy/hazy conditions in the region may be due to the increased anthropogenic emissions.

**Citation:** Tare, V., et al. (2006), Measurements of atmospheric parameters during Indian Space Research Organization Geosphere Biosphere Program Land Campaign II at a typical location in the Ganga Basin: 2. Chemical properties, *J. Geophys. Res.*, *111*, D23210, doi:10.1029/2006JD007279.

## 1. Introduction

[2] Atmospheric aerosols, produced from various natural and anthropogenic sources, have significant direct radiative impact through absorption and scattering of incoming solar radiation [*Charlson et al.*, 1992; *Haywood and Ramaswamy*, 1998; *Hobbs et al.*, 1997]. They can affect climate indirectly by their effects on clouds, albedo and precipitation [*Corbin et al.*, 2002; *Kaufman et al.*, 1997]. These aerosols are also modifying the photolytic rate of gaseous constituents because of their effect on spectral irradiance [*Dickerson et al.*, 1997]. The direct (on radiation budget of Earth-atmospheric system and optical properties) and indirect effects (on cloud properties) of aerosols are function of their size distribution and chemical composition. Consequently the assessment of aerosol chemical composition as a function of size and time is of crucial importance to understand atmospheric processes such as radiative transfer, cloud droplet nucleating ability, acidification, precipitation chemistry and dry deposition.

[3] The composition of the aerosol depends on the source region and it changes with the meteorological conditions in the course of the year. The magnitude and sign of the direct radiative effect of the composite aerosols depend on the relative proportions of different absorbing and scattering species. The results from Indian Ocean Experiment (INDOEX) showed that the pollutants migrating from the Indian subcontinent and southeast Asia to the surrounding oceanic regions during the winter season cause severe air quality degradation with local, regional and global significance [*Ramanathan et al.*, 2001; *Lelieveld et al.*, 2001].

[1]Department of Civil Engineering, Indian Institute of Technology, Kanpur, India.


0148-0227/06/2006JD007279$09.00

**Table 1a.** Details of Samplers and Sampling Duration

| Sampler Type and Model | Particle Size | Flow Rate | Sampling Days | Sampling Duration |
|---|---|---|---|---|
| $PM_{10}$ high-volume sampler (APM 450 Envirotech) | aerodynamic diameter (d) $\leq$ 10.0 $\mu$m | 0.7 to 1.1 $m^3$ $min^{-1}$ | 1–29 Dec 2004 | 0900–1700 local time (8 hours) |
| $PM_{10}$ four-stage cascade impactor (Pacwill Tisch Environmental USA) | stage 1 (d $\leq$ 0.49 $\mu$m), stage 2 (0.49 < d $\leq$ 0.95 $\mu$m), stage 3 (0.95 < d $\leq$ 3.0 $\mu$m), stage 4 (3.0 < d $\leq$ 10.0 $\mu$m) | 1.13 $m^3$ $min^{-1}$ | 25 Dec 2004 to 7 Jan 2005 except on 28 and 29 Dec | 24 hours |
| Aethalometer (AE-21-ER, Magee Scientific, USA) | total suspended black carbon particulate matter | 3.2 L $min^{-1}$ | 1–31 Dec 2004 | 24 hours |

Size-segregated chemical composition of aerosols during INDOEX was used to characterize air masses coming from different source regions [*Gabriel et al.*, 2002] and to estimate the radiative effects of aerosols [*Satheesh et al.*, 1999, 2002] in the oceanic regions. However, scarce information is available concerning aerosol chemical composition in the Indian region [*Kulshrestha et al.*, 1998; *Parmar et al.*, 2001a; *Venkataraman et al.*, 2002; *Alfaro et al.*, 2003]. Further the simultaneous measurements of aerosol physical and optical properties along with the chemical properties are lacking. Size-segregated chemical composition of aerosols is of vital importance in apportioning aerosol loading to different sources/regions.

[4] Sensing the need for collocated and comprehensive measurements, land campaigns were initiated by Indian Space Research Organization Geosphere Biosphere Program (ISRO-GBP) in 2004. The first campaign was conducted during February–March 2004 in the peninsular India [*Moorthy et al.*, 2005]. The second one (LC II) was specially focused on the Ganga Basin in the Northern India during the winter time (December 2004), where enhanced aerosol loads having significant implications to the regional radiative forcing has been found [*Chu et al.*, 2003; *Girolamo et al.*, 2004; *Dey et al.*, 2006; *Ramanathan and Ramana*, 2005; *Tripathi et al.*, 2005a, 2005b]. Details regarding the campaign duration and its objectives are available in a companion paper [*Tripathi et al.*, 2006].

[5] The principal goal of the research work presented in this and the companion paper was to test the hypothesis that anthropogenic aerosol loading significantly contributes to the prolonged and enhanced foggy/hazy winters in plains of Ganges basin. The companion paper reveals that fine/accumulation mode aerosol loading is higher during the foggy/hazy days compared to clear days. This paper delineates chemical characteristics of the aerosols with the aim of broadly determining the significance of regional anthropogenic factors in the enhanced aerosol loadings during foggy/hazy conditions.

## 2. Sampling Site and Methodology

[6] The site typically represents the plains of Ganges basin in the northern part of India (80°20′E and 26°26′N). The sampling was done on the roof of a three storey building in the campus of the Indian Institute of Technology Kanpur, a premier academic institute in India, at a height of about 12m above the ground level. The site is mostly surrounded by vegetation and agricultural fields. The city of Kanpur is on the southwest, and mostly on the downwind side. The meteorological conditions, prevailing during the sampling period, are presented by *Tripathi et al.* [2006].

[7] Single stage $PM_{10}$ aerosol samples were collected on Whatmann GF/A filter papers of size 8″ * 10″ using APM 450 Envirotech High-volume $PM_{10}$ sampler, operated at a flow rate of 0.7–1.1 $m^3$ $min^{-1}$. Stage-separated aerosol samples were collected using a cascade impactor (Pacwill Tisch Environmental, USA) sampler in four stages, at a flow rate of 1.13 $m^3$ $min^{-1}$. Quartz substrates (Tisch Environmental, USA) were used in all stages of sampler except in the first stage, in which Whatmann GF/A filter papers of size 8″ * 10″ were used. An Aethalometer (model AE-21-ER, Magee Scientific, USA) was used to measure the in situ BC concentrations. Details of samplers and sampling duration are given in Table 1a and the analysis techniques of chemical species with their size ranges are summarized in Table 1b.

[8] All filter papers, used for the sampling, were subjected to 24 hour desiccation in a desiccator, to remove the moisture content absorbed by filter papers before and after sampling. The desiccated filter papers were weighted using APM 440, Metler Balance with 10 $\mu$g least count. The extraction procedure prescribed by *Lazaridis et al.* [1999] was followed for estimating water soluble fraction. Filter papers were cut into small pieces and extracted in 40 ml deionized water, using Ultrasonicator for 45 min. The extracted sample was filtered through 0.22 micron filter paper to remove insoluble matter. The concentrations of water soluble anions $Cl^-$, $NO_3^-$ and $SO_4^{2-}$ were determined by Metrohm 761 Compact Ionic Chromatograph (IC) using an electrolyte solution 1.3 mmol $L^{-1}$ $Na_2CO_3$ and 2.0 mmol $L^{-1}$ $Na_2HCO_3$ at a flow rate of 0.7 ml $min^{-1}$ as an eluent and 20 mN $H_2SO_4$ as regenerant. Cations $Na^+$, $K^+$, $Ca^{2+}$and $Mg^{2+}$ were analyzed by Varian SpectrAA 220FS Atomic Absorption Spectrophotometer (AAS) and $NH_4^+$ ion was analyzed by Indophenol blue method using Varian UV spectrophotometer.

**Table 1b.** Details of Analysis Techniques and Size Range

| Analysis Techniques | Components | Size Range, $\mu$m |
|---|---|---|
| Water soluble ions | | |
| Ionic chromatograph (IC) | anions ($Cl^-$, $NO_3^-$, $SO_4^{2-}$) | <10 |
| Atomic absorption spectroscopy (AAS) | cations ($Na^+$, $K^+$, $Ca^{2+}$, $Mg^{2+}$) | <10 |
| Indophenol method | $NH_4^+$ | <10 |
| Acid soluble metals | | |
| Atomic absorption spectroscopy (AAS) | Al, Ca, Fe | <10 |

**Table 2.** Effective Cutoff Diameter (ecd) of Each Stage of Sampler

| Stage | 50% ecd, $\mu$m | $\Delta\log_e D_p$[a] |
|---|---|---|
| 1 | 0.10 | 1.589 |
| 2 | 0.49 | 0.662 |
| 3 | 0.95 | 1.150 |
| 4 | 3(<10) | 1.204 |

[a] $\Delta\log_e D_p = \log_e D_{pn-1} - \log_e D_{pn}$; $D_{pn}$ is the value of 50% ecd of stage n.

[9] For the analysis of soil-derived metals such as Al, Fe and Ca, which are basically acid soluble fractions, hot acid extraction procedure [*U.S. Environmental Protection Agency*, 1999] was followed. Samples were extracted in 25 ml of extraction solution (5.55% $HNO_3$/16.75% HCl) prepared in deionized water. Further, this extraction solution is digested on hot plate at temperature ~170°C for 25–30 min. These digested samples were filtered through 0.22 micron filter paper and later were analyzed by AAS. For quality assurance, 5% of the total number of samples was analyzed for background concentration in the same manner. These blank readings were subtracted from sample readings to get the actual concentrations.

## 3. Results and Discussions

[10] The results of the chemical analysis of aerosols are presented and discussed in three parts. The first part describes the chemical composition of aerosols highlighting presence of certain chemical species in groups or pairs using statistical analysis to explore source and/or formation of such aerosols. The second part attempts to synthesize information related to the plausible chemical reactions in the atmosphere that could be responsible for enhanced aerosol loadings in the region in light of the chemical analysis of the aerosols obtained in the first part and relevant literature. The third part compares the chemical characteristics of the aerosols on foggy/hazy days with clear days in order to validate the hypothesis made for the enhanced foggy/hazy conditions in the winter.

### 3.1. Part I: Chemical Analysis of Aerosols

[11] The monthly average mass concentrations of total particulate matter of size less than 10 $\mu$m ($PM_{10}$), and ions such as $NO_3^-$, $SO_4^{2-}$, $Cl^-$, $NH_4^+$, $Na^+$, $K^+$, $Ca^{2+}$ and $Mg^{2+}$ in the aerosol samples collected for approximately 8 hours in a day on every day over a month-long land campaign period were found to be 203.4 ± 39.9, 15.7 ± 5.58, 14.9 ± 3.3, 3.1 ± 0.1, 8.76 ± 4.3, 4.34 ± 0.1, 5.0 ± 0.7, 1.6 ± 0.6 and 0.23 ± 0.05 $\mu$g $m^{-3}$ respectively. The measured total water soluble ionic fraction contributed to approximately 34% of the total mass of aerosol of which cations and anions account for 29% and 71% respectively. $SO_4^{2-}$ and $NO_3^-$ contribute to approximately 62% of anionic species by weight while $NH_4^+$ and $K^+$ contribute to approximately 69% of cationic species by weight.

[12] The concentrations of non-sea-salt potassium (nss-$K^+$) and non-sea-salt sulfate (nss-$SO_4^{2-}$) were calculated as nss-$K^+ = [K^+]_{measured} - [Na^+] \times 0.037$ [*Venkataraman et al.*, 2002; *Hitchcock et al.*, 1980] and nss-$SO_4^{2-} = [SO_4^{2-}]_{measured} - [Na^+] \times 0.2516$ [*Cheng et al.*, 2000; *Millero and Sohn*, 1992], respectively. The monthly average concentrations of nss-$K^+$ and nss-$SO_4^{2-}$ were found to be 5.04 ± 0.95 and 14.54 ± 5.13 $\mu$g $m^{-3}$ respectively. These higher concentrations of nss-components indicate the incorporation of nonmarine aerosols.

[13] The monthly average concentrations of the acid soluble metals *viz.* Al, Fe and Ca in $PM_{10}$ mass were found to be 1.1 ± 0.4, 2.1 ± 0.6, and 1.9 ± 0.7 $\mu$g $m^{-3}$ respectively, which contributed to 2.5% of the total mass of aerosol. Much of the calcium in the aerosol mass (approximately 85%) was water soluble. BC contributes to ~10% of $PM_{10}$ [*Tripathi et al.*, 2005a]. The rest of the mass (~35%) could be attributed to the unmeasured organics and other metals. The organic carbon content in the total mass of the particulate matter was estimated to be ~22% from the OC/BC ratio retrieved from AERONET measurements during the winter in Kanpur [*Dey et al.*, 2006].

[14] The chemical analysis of $PM_{10}$ mass suggests that much of the aerosol mass could be attributed to the species/constituents (e.g., $K^+$, $NH_4^+$, $NO_3^-$, $SO_4^{2-}$, $HCO_3^-$, BC) which could plausibly be linked to the anthropogenic emission sources (mostly burning of fossil fuel and biomass) within the region. As such it may be inferred that enhanced aerosol loading in the region could be attributed to the anthropogenic factors. In order to gain further insight on the enhanced aerosol loading due to anthropogenic factors, chemical analysis of the size segregated aerosol samples collected simultaneously using a four-stage cascade impactor was carried out. The effective cutoff diameter (ecd) of each stage is given in Table 2, where the ranges are $d < 0.49$ $\mu$m, $0.49 < d < 0.95$ $\mu$m, $0.95 < d < 3$ $\mu$m and $3 < d < 10$ $\mu$m for the first, second, third and fourth stages respectively. The first two stages are considered as the fine mode and the last two as the coarse mode. Since a cut size of 1.0 $\mu$m was not available in cascade sampler $PM_{10}$ sampler, the cut size of 0.95 $\mu$m is chosen to separate the particles in fine and coarse mode. The daily total mass concentration varied in the range 163.84–326.74 $\mu$g $m^{-3}$ and much of the aerosols were of fine mode (approximately 81% aerosol mass in the size range 0.1–0.95 $\mu$m.

[15] A summary of the results on loading of water soluble fraction of various chemical species for size segregated aerosols is presented in Table 3. Graphical representation (refer to Figure 1) of the chemical species/constituents in the aerosol samples collected from the four stages reveal that (1) water soluble cations $NH_4^+$ and $K^+$ are significantly higher in the first three stages, i.e., in the finer fraction; (2) water soluble cations $Ca^{2+}$ and $Mg^{2+}$ and acid soluble metals (Al, Ca and Mg) are higher in the coarser fraction; and (3) significant fraction of the water soluble anionic species consists of $NO_3^-$ and $SO_4^{2-}$ in all sizes. A further analysis of the mass size distributions of aerosols and their water soluble components as per the method used by *Satoshi* [1976] is presented in Figures 2a–2i. All mass size distributions are found to be unimodal with the dominant peak in the accumulation mode except for $Ca^{2-}$ and $Mg^{2+}$ ions in the water soluble fraction. These results further support the argument that much of the enhanced aerosol loading at the sampling site could be attributed to the anthropogenic sources, namely burning of fossil fuel and biomass.

**Table 3.** Minimum, Maximum, and Average Concentration of Major Ionic Components in Each Stage of the Four-Stage Cascade $PM_{10}$ Sampler

| Component | Concentration, $\mu g\ m^{-3}$, First Stage ($d \leq 0.49\ \mu m$) | | | Concentration, $\mu g\ m^{-3}$, Second Stage ($0.49 < d \leq 0.95\ \mu m$) | | | Concentration, $\mu g\ m^{-3}$, Third Stage ($0.95 < d \leq 3.0\ \mu m$) | | | Concentration, $\mu g\ m^{-3}$, Fourth Stage ($3.0 < d \leq 10.0\ \mu m$) | | |
|---|---|---|---|---|---|---|---|---|---|---|---|---|
| | Minimum | Maximum | Average | Minimum | Maximum | Average | Minimum | Maximum | Average | Minimum | Maximum | Average |
| Mass concentration | 56.93 | 109.97 | 88.86 ± 21.18 | 41.21 | 216.78 | 114.29 ± 57.6 | 24.37 | 63.23 | 37.61 ± 12.43 | 3.73 | 13.11 | 8.11 ± 3.2 |
| $Cl^-$ | 1.17 | 2.52 | 1.79 ± 0.50 | 1.30 | 5.09 | 2.96 ± 1.11 | 0.32 | 1.25 | 0.67 ± 0.26 | 0.05 | 0.22 | 0.11 ± 0.05 |
| $NO_3^-$ | 4.37 | 11.05 | 7.68 ± 2.1 | 7.69 | 33.22 | 19.14 ± 8.88 | 2.33 | 9.30 | 5.20 ± 2.0 | 0.46 | 1.21 | 0.73 ± 0.24 |
| $SO_4^{2-}$ | 3.41 | 6.99 | 5.04 ± 1.03 | 5.76 | 23.83 | 12.86 ± 6.44 | 1.56 | 7.22 | 3.41 ± 1.77 | 0.24 | 0.81 | 0.42 ± 0.15 |
| $NH_4^+$ | 3.13 | 6.24 | 4.53 ± 0.94 | 6.79 | 18.73 | 12.47 ± 4.11 | 2.83 | 8.66 | 4.81 ± 1.92 | 0.10 | 0.35 | 0.20 ± 0.07 |
| $Na^+$ | 0.83 | 1.18 | 1.02 ± 0.11 | 0.05 | 0.22 | 0.15 ± 0.05 | 0.02 | 0.16 | 0.06 ± 0.04 | 0.01 | 0.1 | 0.04 ± 0.33 |
| $K^+$ | 1.67 | 2.86 | 2.33 ± 0.42 | 1.37 | 5.92 | 2.99 ± 1.31 | 0.27 | 1.50 | 0.71 ± 0.37 | 0.07 | 0.17 | 0.10 ± 0.04 |
| $Mg^{2+}$ | 0.02 | 0.05 | 0.03 ± 0.01 | 0.03 | 0.06 | 0.04 ± 0.01 | 0.09 | 0.23 | 0.14 ± 0.04 | 0.03 | 0.09 | 0.05 ± 0.02 |
| $Ca^{2+}$ | 0.05 | 0.27 | 0.13 ± 0.08 | 0.09 | 0.23 | 0.16 ± 0.05 | 0.23 | 0.82 | 0.53 ± 0.15 | 0.15 | 0.38 | 0.22 ± 0.08 |
| nss-$K^+$ | 1.46 | 2.81 | 2.28 ± 0.45 | 1.36 | 5.92 | 2.97 ± 1.38 | 0.26 | 1.56 | 0.8 ± 0.45 | 0.03 | 0.17 | 0.09 ± 0.04 |
| nss-$SO_4^{2-}$ | 2.62 | 6.75 | 4.73 ± 1.11 | 5.74 | 23.79 | 12.68 ± 6.82 | 1.55 | 7.21 | 3.69 ± 1.86 | 0.28 | 0.79 | 0.42 ± 0.15 |

#### 3.1.1. Correlation Analysis

[16] An empirical approach to arrive at the sources of aerosols could be to examine the paired association of water soluble chemical constituents. The use of correlation coefficients allows a quantitative estimate of the similarity of the variations of any two species. Highly correlated species may come from the similar sources. Tables 4a and 4b present the matrix of coefficient of correlation values for fine and coarse mode aerosols, respectively to identify the paired association of water soluble chemical constituents of the size segregated aerosols collected at the sampling site. The statistical analysis of the data presented in Table 4a suggests that $NH_4^+$-$NO_3^-$, $NH_4^+$-$SO_4^{2-}$, $NH_4^+$-$Cl^-$, $SO_4^{2-}$-$NO_3^-$, $SO_4^{2-}$-$Cl^-$, $NO_3^-$-$Cl^-$, $K^+$-$Cl^-$, and $Ca^{2+}$-$Mg^{2-}$ possibly have the same source/origin or sources/origins that contribute together for their presence in the aerosol mass of fine mode particles. Black carbon is also moderate to highly correlated with water soluble chemical constituents ($NO_3^-$, $SO_4^{2-}$, $NH_4^+$, $K^+$ and $Cl^-$) suggesting its anthropogenic origin. Particularly, moderate correlation (0.334) between BC and fine mode $K^+$ suggests that BC has also some other source besides biomass burning, as fine mode $K^+$ can be considered as biomass tracer [*Andreae and Merlet*, 2001; *Y. Ma et al.*, 2003].

[17] In the coarse mode (refer to Table 4b), $Mg^{2+}$-$NO_3^-$, $K^+$-$NO_3^-$, $Mg^{2+}$-$SO_4^{2-}$, $K^+$-$SO_4^{2-}$, $Mg^{2+}$-$Cl^-$, $NH_4^+$-$K^+$ also indicate strong paired association. These components are also highly correlated with the fine mode particulate matters having aerodynamic diameters less than $\sim$1 $\mu$m indicating their anthropogenic origin. In contrast, soil derived components, e.g., $Mg^{2+}$ and $Ca^{2+}$, are highly correlated with the coarse mode particulate matters having aerodynamic diameters greater than $\sim$1 $\mu$m but less than 10 $\mu$m. On the other hand, $Na^+$ is not correlated with any of the other constituents in fine and coarse mode.

#### 3.1.2. Correlation Matrix and Factor Analysis

[18] Factor analysis [*Harman*, 1960; *Rencher*, 2002] was also used to deduce interrelationships between the measured atmospheric particulates. In recent years, factor analysis has been successfully applied for data reduction in aerosol studies. Factor extraction using principal component method, orthogonal varimax rotation with eigen values $\geq$1 (as a cutoff value) has been done by utilizing the principal component loading. The principal component loading can be obtained by multiplying square root of eigen values with their respective eigen vectors. The factor loading for fine mode correspond to three eigen values 5.6069, 2.3212, 1.1072 and for coarse mode correspond to two eigen values 6.1071 and 1.4156.

[19] Table 4c presents factor loading for fine mode aerosols, which accounts for 90% of the total variance. Factor 1, which accounts for 56% of the total variance, reveals significant contributions of $NO_3^-$, $SO_4^{2-}$, $Cl^-$, $NH_4^+$, $K^+$ and BC in the mass of fine particles suggesting that these particles are plausibly originate from biomass and fossil fuel burning. Factor 2, accounting for 23% of the total variance, indicates that soil derived components ($Mg^{2+}$ and $Ca^{2+}$) also contribute to the fine mode particles. Factor 3 which accounts for vary small part of the total variance (11%), shows higher loading for $Na^+$ suggesting that a small portion of fine particulates may be made of salts through long-range transport or inland water bodies within the

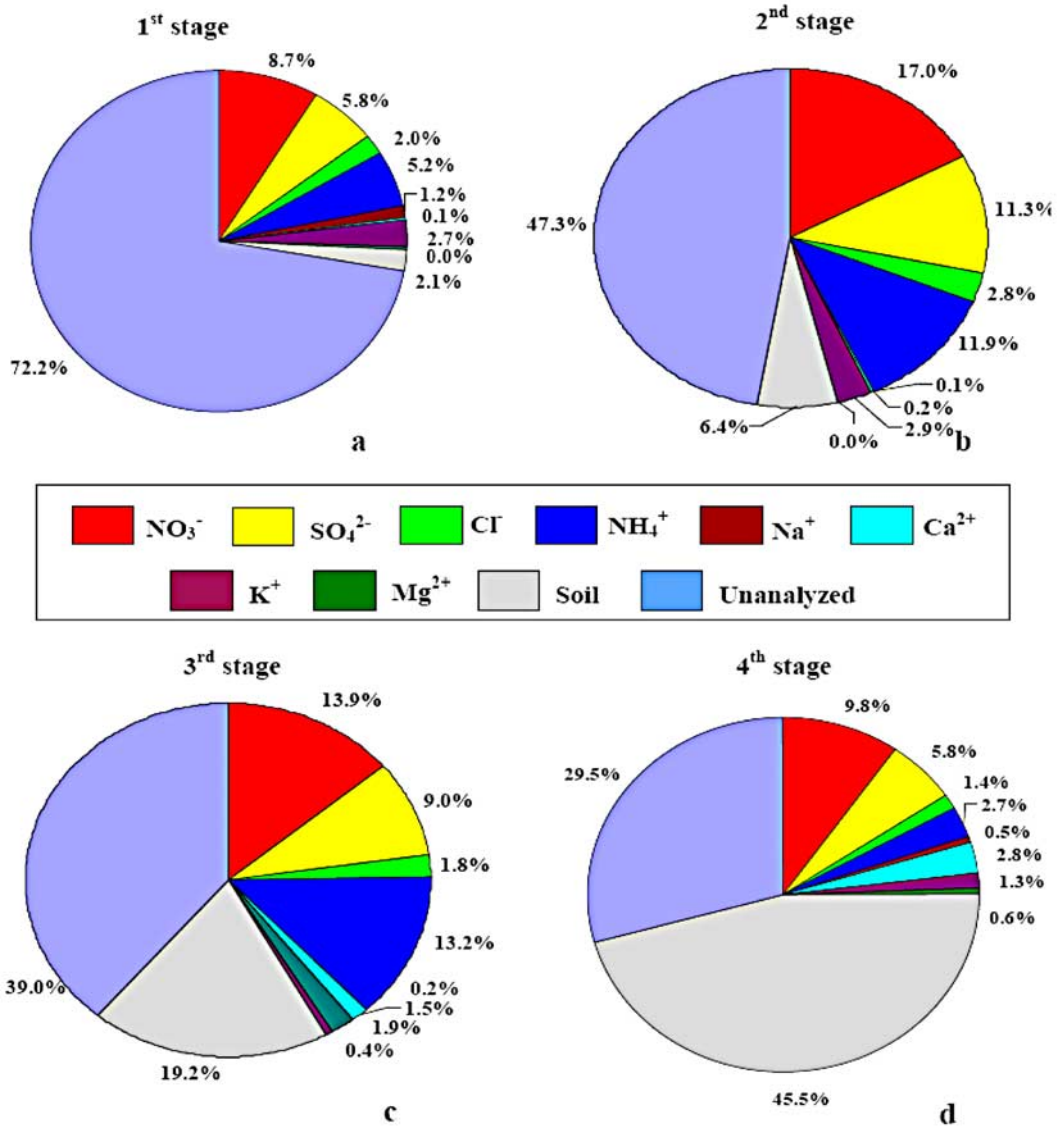


**Figure 1.** (a–d) Percentage contribution of each chemical component in each stage of the four-stage cascade impactor.

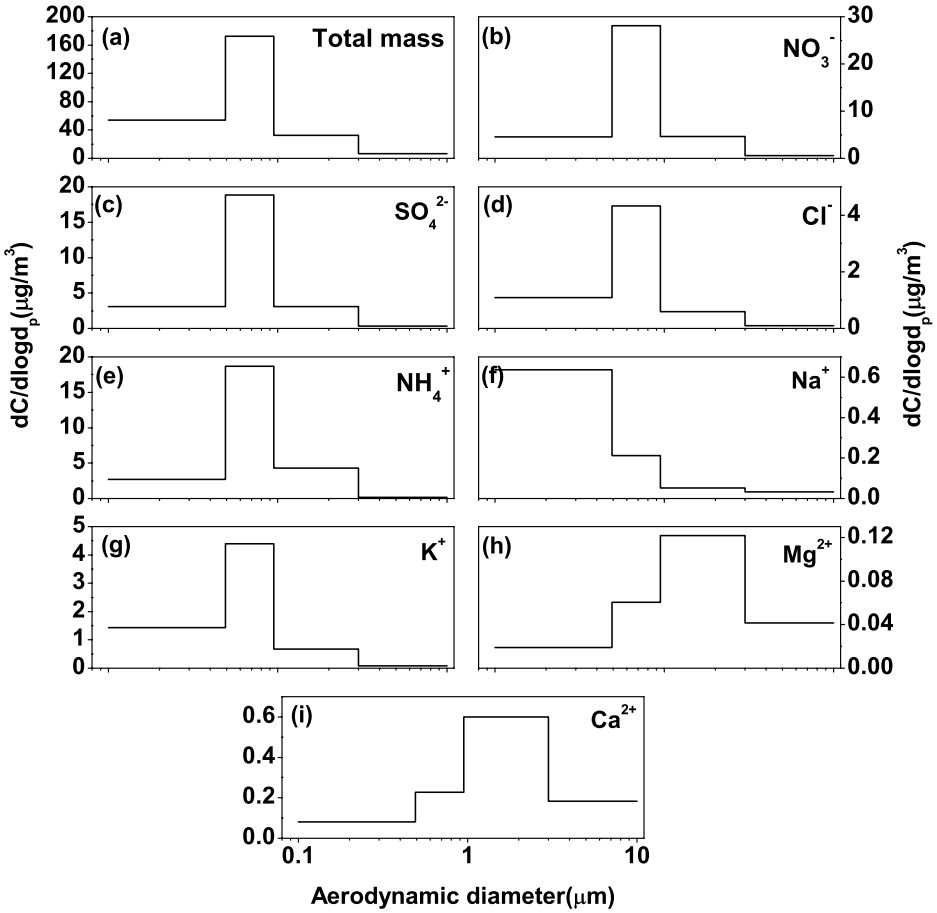


**Figure 2.** (a–i) Mass size distribution of total mass of aerosol and its major ions. Note different ranges of values in the *y* axis of each graph.

region. On the other hand, factor loading for the coarse mode particles (Table 4d) reveals that major portion of these aerosols is of soil origin (61% of the total variance accounted by factor 1 with high loading of Ca and Mg). Interestingly, a small portion of the coarse aerosols accounting for 14% of the total variance suggest contribution from the tracers of biomass/fossil fuel burning and agricultural activities (moderate loadings of $NH_4^+$, $K^+$ and $Ca^{2+}$ in factor 2, Table 4d).

### 3.1.3. Relative Contribution of Different Sources

[20] Attempt has been made to estimate the relative contribution of different probable sources to the measured aerosols at each stage (Figure 3). Considering Al to be 8% of the soil mass [*Uehara*, 2005; *Sudesh and Rajamani*, 2004] and reconstructing the mass of soil-derived components, their contribution becomes 2.1, 6.4, 19.2 and 45.5% in each stage of the cascade impactor respectively. Another major source of emissions in the region is biomass burning. For quantifying the biomass contribution, emission factor values of PM and K reported in the literature have been considered [*Andreae and Merlet*, 2001]. The monthly mean values of total biomass burnt in the western part of the Ganga basin, in which the present monitoring site is located, during the winter season [*Venkataraman et al.*, 2006] have

**Table 4a.** Correlation Matrixes in the Fine Mode

| | PM | $NO_3^-$ | $SO_4^{2-}$ | $Cl^-$ | $NH_4^+$ | $Na^+$ | $Mg^{2+}$ | $K^+$ | $Ca^{2+}$ | BC |
|---|---|---|---|---|---|---|---|---|---|---|
| PM | 1.000 | 0.915 | 0.950 | 0.833 | 0.921 | 0.077 | 0.390 | 0.660 | −0.011 | 0.788 |
| $NO_3^-$ | 0.915 | 1.000 | 0.934 | 0.717 | 0.966 | −0.129 | 0.290 | 0.512 | −0.143 | 0.660 |
| $SO_4^{2-}$ | 0.950 | 0.934 | 1.000 | 0.712 | 0.961 | −0.014 | 0.274 | 0.491 | −0.210 | 0.832 |
| $Cl^-$ | 0.833 | 0.717 | 0.712 | 1.000 | 0.720 | 0.243 | 0.133 | 0.609 | −0.032 | 0.707 |
| $NH_4^+$ | 0.931 | 0.966 | 0.961 | 0.720 | 1.000 | −0.016 | 0.245 | 0.536 | −0.183 | 0.715 |
| $Na^+$ | 0.077 | −0.129 | −0.014 | 0.243 | −0.016 | 1.000 | 0.092 | 0.321 | 0.342 | 0.054 |
| $Mg^{2+}$ | 0.390 | 0.290 | 0.274 | 0.133 | 0.245 | 0.092 | 1.000 | 0.517 | 0.796 | −0.077 |
| $K^+$ | 0.660 | 0.512 | 0.491 | 0.609 | 0.536 | 0.321 | 0.517 | 1.000 | 0.454 | 0.334 |
| $Ca^{2+}$ | −0.011 | −0.143 | −0.210 | −0.032 | −0.183 | 0.342 | 0.796 | 0.454 | 1.000 | −0.465 |
| BC | 0.788 | 0.660 | 0.832 | 0.707 | 0.715 | 0.054 | −0.077 | 0.334 | −0.465 | 1.000 |

**Table 4b.** Correlation Matrixes in the Coarse Mode

| | PM | $NO_3^-$ | $SO_4^{2-}$ | $Cl^-$ | $NH_4^+$ | $Na^+$ | $Mg^{2+}$ | $K^+$ | $Ca^{2+}$ |
|---|---|---|---|---|---|---|---|---|---|
| PM | 1.000 | 0.77 | 0.626 | 0.703 | 0.448 | 0.451 | 0.929 | 0.502 | 0.809 |
| $NO_3^-$ | 0.770 | 1.000 | 0.913 | 0.933 | 0.711 | 0.323 | 0.908 | 0.793 | 0.486 |
| $SO_4^{2-}$ | 0.626 | 0.913 | 1.000 | 0.850 | 0.864 | 0.344 | 0.769 | 0.881 | 0.353 |
| $Cl^-$ | 0.703 | 0.933 | 0.850 | 1.000 | 0.578 | 0.205 | 0.881 | 0.637 | 0.598 |
| $NH_4^+$ | 0.448 | 0.711 | 0.864 | 0.578 | 1.000 | 0.321 | 0.577 | 0.959 | 0.197 |
| $Na^+$ | 0.451 | 0.323 | 0.344 | 0.205 | 0.321 | 1.000 | 0.418 | 0.477 | 0.351 |
| $Mg^{2+}$ | 0.929 | 0.908 | 0.769 | 0.881 | 0.577 | 0.418 | 1.000 | 0.650 | 0.769 |
| $K^+$ | 0.502 | 0.793 | 0.881 | 0.637 | 0.959 | 0.477 | 0.650 | 1.000 | 0.214 |
| $Ca^{2+}$ | 0.809 | 0.486 | 0.353 | 0.598 | 0.197 | 0.351 | 0.769 | 0.214 | 1.000 |

been used to estimate the percentage of K in the emissions from biomass burning in the region. This value has been subsequently used to estimate the relative contribution of biomass burning to the total aerosols mass at each stage. The error estimate of the emission factors of components emitted from biomass burning are discussed in details in *Venkataraman et al.* [2006]. The contribution of biomass burning is much higher in the fine mode (first and second stages) than in the coarse mode (third and fourth stages). Third major source is the gas-phase reactions through which the secondary water-soluble aerosols form in the atmosphere. The contribution of the gas-phase reactions is highest (31.2%) in the second stage. Unanalyzed part varies between 18 (fourth stage) to 39% (first stage). BC, OC and organic matter are the most probable components expected to fill the unanalyzed portion. BC and OC generally exist in the fine mode, which corresponds to the fact that the unanalyzed part is higher in fine mode than that in coarse mode.

### 3.2. Part II: Plausible Atmospheric Reactions and Mechanisms for Observed Chemical Analysis of Aerosol Samples

[21] In this part, an attempt is made to synthesize information related to the plausible chemical reactions in the atmosphere that could be responsible for enhanced aerosol loadings in the region in light of the chemical analysis of the aerosols obtained in the first part on the basis of available relevant literature reports.

#### 3.2.1. Nitrate

[22] $NO_3^-$ can be found in the atmosphere both in the fine and coarse mode with highly variable amount, the larger particles are generally associated with marine region and the finer particles are associated with a polluted urban region [*Finlayson-Pitts and Pitts*, 2000]. The mass size distribution curve for water soluble $NO_3^-$ over a polluted urban region of Kanpur, where marine source of origin of $NO_3^-$ are unlikely to contribute, is shown in Figure 2b. Much of the water soluble (≈81%) nitrate is obtained from fine mode aerosols with one major peak in 0.49–0.95 $\mu$m range. It can be observed that the average water soluble $NO_3^-$ loading varied in the range 0.73 to 19.14 $\mu g\ m^{-3}$ of aerosol mass collected for various size ranges of the aerosol with maximum loading in the size range 0.49 to 0.95 $\mu$m, i.e., in the fine mode (refer to Table 3). Nitrates may be formed by the homogeneous gas–phase transformations of $NO_x$ to $HNO_3$, which in tern may react with ammonia gas to form ammonium nitrate, or with preexisting fine particles [*Satoshi*, 1976; *Zhuang et al.*, 1999; *Parmar et al.*, 2001a; *J. Ma et al.*, 2003]. Accurate and artifact-free determination of $NO_3^-$ in particles is much more difficult than the determination of $SO_4^{2-}$ because both positive and negative artifact can occur [*Finlayson-Pitts and Pitts*, 2000].

$$NH_3(g) + HNO_3(g) \Leftrightarrow NH_4NO_3(aq\ or\ s) \quad (1)$$

[23] The reactions in which $HNO_3$ may replace water-soluble organic particulates, e.g., formate, acetate and oxalate through the reaction

$$(NH_4)_2C_2O_4(aq) + 2HNO_3(g) \Leftrightarrow 2NH_4NO_3(aq\ or\ s) + C_2H_2O_4 \quad (2)$$

are also important pathways for presence of nitrates in substantial quantities in particles [*Tabazadeh et al.*, 1998; *J. Ma et al.*, 2003]. The organic ligands mentioned above

**Table 4c.** Factor Analysis for Fine Mode Particles

| | Factor 1 | Factor 2 | Factor 3 |
|---|---|---|---|
| PM | 0.9915 | −0.0391 | −0.0367 |
| $NO_3^-$ | 0.9312 | 0.1108 | −0.2366 |
| $SO_4^{2-}$ | 0.9595 | 0.1576 | −0.1010 |
| $Cl^-$ | 0.8476 | −0.0081 | 0.2990 |
| $NH_4^+$ | 0.9495 | 0.1270 | −0.1163 |
| $Na^+$ | 0.0911 | −0.4461 | 0.8357 |
| $Mg^{2+}$ | 0.3347 | −0.8009 | −0.4052 |
| $K^+$ | 0.6710 | −0.5459 | 0.1343 |
| $Ca^{2+}$ | −0.0602 | −0.9809 | −0.0925 |
| BC | 0.8005 | 0.4073 | 0.2179 |

**Table 4d.** Factor Analysis for Coarse Mode Particles

| | Factor 1 | Factor 2 |
|---|---|---|
| PM | 0.8659 | 0.4025 |
| $NO_3^-$ | 0.9492 | −0.1089 |
| $SO_4^{2-}$ | 0.9043 | −0.3526 |
| $Cl^-$ | 0.8956 | 0.0415 |
| $NH_4^+$ | 0.7590 | −0.5728 |
| $Na^+$ | 0.4845 | 0.0689 |
| $Mg^{2+}$ | 0.9564 | 0.2392 |
| $K^+$ | 0.8180 | −0.5289 |
| $Ca^{2+}$ | 0.6623 | 0.6738 |

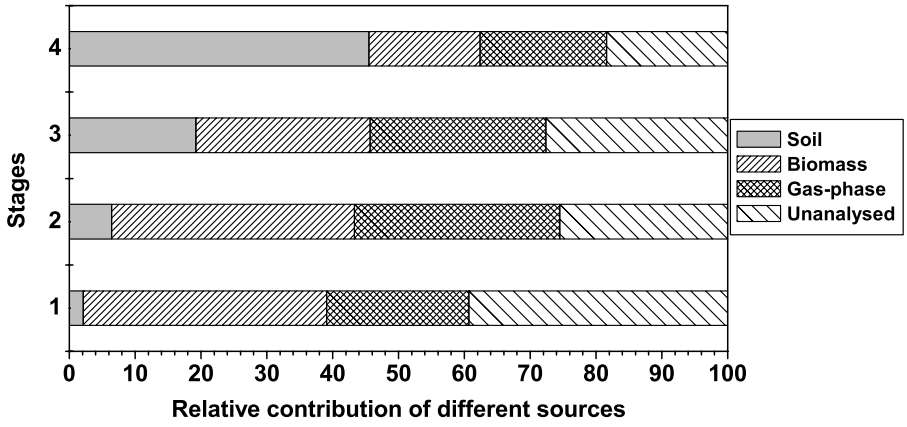


**Figure 3.** Relative contribution of different probable sources to the measured aerosols at each stage.

can be abundant in fine particles, such as those originating from biomass burning [*Andreae et al.*, 1988; *Talbot et al.*, 1988]. In this study species such as formate, acetate and oxalate were not analyzed. The reaction (1) is important only when $NH_4^+$ is excess in comparison with $SO_4^{2-}$ in the particles. The molar ratios of $NH_4^+$ to $SO_4^{2-}$ and $NO_3^-$, in both fine and coarse modes, indicate excess availability of ammonium. Because $NH_4NO_3$ is a highly volatile species, it can be only formed and remain stable in particulate phase when the product of gas-phase concentrations of ammonia and nitric acid $[NH_3]$ $[HNO_3]$ ($ppb^2$) in the air exceeds the equilibrium product for the reaction (1) [*Seinfeld and Pandis*, 1998]. High relative humidity and lower air temperatures are also preferred conditions for the formation of $NH_4NO_3$ [*Hillamo and Kauppinen*, 1991; *Nadstazik et al.*, 2000; *Lewandowska et al.*, 2004].

[24] The major source of ammonia gas in this region could be agricultural fields, which are situated on upwind side of the sampling location. Observed average vapor phase $NH_3$ concentration at some locations in the region (Ganges basin) during the winter months was typically high: 30.33 ppbv in Kanpur [*Kishore*, 2005], 11.8 ppbv in Agra [*Parmar et al.*, 2001b] and 47.3 ppbv in Delhi [*Kapoor et al.*, 1992]. No data regarding the concentration of $HNO_3$ in the gas phase was available during the sampling period. However, the average concentration of $HNO_3$ in the gas phase in the month of February was estimated to be 0.8 ppbv [*Kishore*, 2005]. In the month of December (sampling period in the present study) $HNO_3$ in the gas phase could lower because of lower incoming solar radiations. Assuming even 50% concentration of gaseous phase $HNO_3$ in the month of December compared to that measured in February at the same location, the product of the gas-phase concentrations of $[NH_3]$ and $[HNO_3]$ would be $\sim$12.13 $ppb^2$. The monthly average dissociation constant ($K_p$) for reaction (2) was found to be 2.03 $ppb^2$, which is much less than the product of the gas phase concentration of $[NH_3]$ and $[HNO_3]$. Thus high levels of both $NH_3$ and $HNO_3$ associated with favorable environmental conditions (e.g., high relative humidity: 69–93% and lower temperature: 8°–16°C) during December/January in the region is expected to support the formation of particulate $NH_4NO_3$.

[25] Some fraction of the water soluble nitrate ($\approx$19%) is obtained from coarse mode aerosols (0.95–3 $\mu$m). Nitrate laden coarse aerosols can be produced by either the reaction of gaseous nitric acid with sea-salt aerosols (reaction (3)) or with aerosol of soil origin (reactions (4) and (5)).

$$HNO_3(g) + NaCl(aq) \Leftrightarrow NaNO_3(aq) + HCl(g) \quad (3)$$

$$CaCO_3(aq) + 2HNO_3(g) \Leftrightarrow Ca(NO_3)_2(aq) + H_2O + CO_2(g) \quad (4)$$

$$MgCO_3(aq) + 2HNO_3(g) \Leftrightarrow Mg(NO_3)_2(aq) + H_2O + CO_2(g) \quad (5)$$

[26] As availability of sea salt at this site is very low, the major contribution may be due to soil derived particles. During the daytime, nitrates of Ca and Mg may be formed by the reaction of atmospheric $HNO_3$ with airborne soil. Soil surface thus can act as an absorbing solution. Aerosol nitrate may thus be formed by the absorption and subsequent reaction of $NO_2$ on the soil aerosol surface or by dissolution of gaseous $HNO_3$. Soil particles readily act as a sink for nitric acid.

### 3.2.2. Sulfate

[27] The size distribution curve for water soluble $SO_4^{2-}$ loading on the aerosol samples collected in shown in Figure 2c. It can be observed that the average water soluble $SO_4^{2-}$ loading varied in the range 0.42 to 12.86 $\mu g\ m^{-3}$ of aerosol mass collected for various size ranges of the aerosol with maximum loading in the size range 0.49 to 0.95 $\mu$m, i.e., in the fine mode (refer to Table 3). Much of the water soluble sulfate (84.5%) is contributed by the fine mode aerosols.

[28] Formation and size distribution of aerosols with substantial loadings of sulfate have been widely studied. *Hering and Friedlander* [1982] reported sulfate laden aerosols in two modes; condensation mode (0.17–0.25 $\mu$m) and droplet mode (0.6–0.65 $\mu$m). The condensation mode has been ascribed to gas-to-particle transformation of $SO_2$ gas [*Hering and Friedlander*, 1982; *Venkataraman et al.*, 2001]. While the droplet mode sulfate cannot be explained by

**Table 5.** $K_p$ Values for Reaction (6) at Different Temperature and Relative Humidity [*Pio and Harrison*, 1987]

| T, °C | 80% R.H | 90% R.H |
|---|---|---|
| 5 | 0.43 | 0.12 |
| 10 | 1.60 | 0.44 |
| 15 | 5.90 | 1.48 |

primary emissions, gas-phase nucleation or condensation, the possible formation mechanisms of this mode may include growth of the condensation mode of particles or by evaporation of large droplets. Aqueous-phase conversion of dissolved $SO_2$ to $SO_4^{2-}$ by $H_2O_2$, $O_3$ and oxygen (catalyzed by $Fe^{3+}$and $Mn^{2+}$) are predominant pathways for droplet mode sulfate formation, followed by ammonia neutralization [*Saxena and Seigneur*, 1987; *Pandis and Seinfeld*, 1989]. *Meng and Seinfeld* [1994] have suggested that the droplet mode can be formed by the activation of the condensation mode particles to form fog or cloud droplets, followed by aqueous–phase chemical reactions and fog evaporation. On the days of high relative humidity condensation mode may get activated to form fogs and clouds. Significant sulfate can be formed by aqueous-phase reactions in the fog or cloud droplets [*Pandis et al.*, 1992; *Kermein and Wexler*, 1995], leaving the residual droplet mode particles with higher sulfate concentration.

[29] The $SO_4^{2-}$ laden aerosols may also originate from both sea-salt and soil particles. Since the sampling site is an inland site about 1600 km away from the nearest coast, contribution of sea-salt sulfate will be insignificant. Hence in the study region sulfate may be soil derived or formed by the gas-phase sulfur dioxide or sulfuric acid on the wet surface of the basic soil particles. Several studies carried out in the region suggest that $SO_2$ concentrations are generally low despite substantial emissions and that the soil derived aerosols are alkaline in nature [*Sharma et al.*, 2003]. The observed $SO_2$ levels during the study period were also very low (<5 ppmv). Thus it may be argued that sulfate laden aerosols in the region could be essentially due to interaction of $SO_2$ and soil derived aerosols in the atmosphere.

### 3.2.3. Chloride

[30] The size distribution curve for water soluble $Cl^-$ loading on the aerosol samples collected in shown in Figure 2d. It can be observed that the average water soluble $Cl^-$ loading varied in the range 0.11 to 2.96 $\mu$g m$^{-3}$ of aerosol mass collected for various size ranges of the aerosol. No significant variation is observed in water soluble Cl among various size ranges of the aerosol samples collected (refer to Table 3). Water soluble $Cl^-$ in aerosols may be contributed by neutralization of $NH_3$ by HCl. The majority of ambient HCl is emitted from the coal combustion processes and incineration of domestic and industrial waste. *Willison et al.* [1989] and *Kaneyasu et al.* [1999] have found highest concentration of fine mode $Cl^-$ during winter period. The formation of $NH_4Cl$ particles occurs when product of gas-phase concentration of ammonia and hydrochloric acid exceeds equilibrium product ($K_p$) of chemical reaction (6).

$$NH_3(g) + HCl(g) \Leftrightarrow NH_4Cl(\mathrm{s}) \qquad (6)$$

[31] *Pio and Harrison* [1987] studied the effect of temperature and relative humidity on the formation of particulate $NH_4Cl$. They reported the values of $K_p$ (ppb$^2$) at different temperature and relative humidity, which are given in Table 5. However, in this study HCl concentration in the atmosphere could not be measured. Environmental conditions of high relative humidity and low temperature (as observed during this study) may favor the formation of fine mode $NH_4Cl$ particulate. Significant correlation for paired association of $NH_4^+$ and $Cl^-$ suggests this possibility (refer to Tables 4a and 4b). The water soluble $Cl^-$ in coarse mode aerosol may, however, be soil derived (e.g., $MgCl_2$) as significant correlation for paired association between $Mg^{2+}$ and $Cl^-$ is obtained for coarse aerosols (refer to Table 4b).

### 3.2.4. Ammonium

[32] The size distribution curve for water soluble $NH_4^+$ loading on the aerosol samples collected in shown in Figure 2e. It can be observed that the average water soluble $NH_4^+$ loading varied in the range 0.20 to 12.47 $\mu$g m$^{-3}$ of aerosol mass collected for various size ranges of the aerosol with maximum loading in the size range 0.49 to 3.0 $\mu$m (refer to Table 3). Much of the water soluble ($\approx$76.5%) ammonium is obtained from fine mode aerosols. The particulate ammonium, in the condensation mode, may originate from the heteromolecular nucleation of ammonia vapor that reacts with the acidic gases such as $H_2SO_4$, $HNO_3$ and HCl, whereas the particulate ammonium in droplet mode, may originate from condensation or reaction of ammonium gas on an acid particle surface of anthropogenic origin and accumulates in fine mode [*Zhuang et al.*, 1999]. The stability of $NH_4NO_3$, $(NH_4)_2SO_4$, and $NH_4Cl$ is different and depends on the temperature and relative humidity. Ammonium sulfate is most stable while ammonium chloride is most volatile; hence ammonia prefers to react with sulfuric acid or sulfate. First, ammonia reacts irreversibly with sulfate to form ammonium sulfate as shown in reactions (7a) and (7b):

$$NH_3(g) + H_2SO_4(aq) \Leftrightarrow NH_4HSO_4(aq\ or\ s) \qquad (7a)$$

$$NH_3(g) + NH_4HSO_4(aq\ or\ s) \Leftrightarrow (NH_4)_2SO_4(aq\ or\ s) \qquad (7b)$$

[33] When sulfuric acid is completely neutralized, excess ammonia (henceforth referred as free ammonia) can react with nitric acid to form semivolatile ammonium nitrate as shown in reaction (1) [*Gonzalez et al.*, 2003].

[34] Statistically significant correlation for paired association between sulfate and ammonium in the fine mode (Table 4a) also suggests this possibility. The ideal stoichiometric ratios for $NH_4^+/SO_4^{2-}$, $NH_4^+/NO_3^-$ and $NH_4^+/Cl^-$ are 0.37, 0.29 and 0.51 respectively. The observed average stoichiometric ratios for $NH_4^+$ to $SO_4^{2-}$, $NO_3^-$ and $Cl^-$ are 2.73, 2.35 and 8.00 respectively. This indicates that a significant amount of ammonium ions may have been contributed from salts of carbonic acid such as $(NH_4)_2CO_3$ and $NH_4HCO_3$, and salts of organic acids viz., $CH_3COONH_4$ and $HCOONH_4$ [*Parmar et al.*, 2001a]. These may be formed by the reaction of $NH_3$ gas with wet aerosols.

[35] A small fraction of water soluble ammonium (≈13.5%) is also contributed by the coarse mode aerosols. There is no known major emission source for the coarse mode ammonium. The agglomeration of fine mode ammonium particles onto the coarse mode particles is also unlikely. Several workers [*Savoie and Prospero*, 1982; *Wall et al.*, 1988; *Zhuang et al.*, 1999] have observed coarse mode ammonium in aerosol. They have attributed its formation by reaction of $NH_3$ gas on sulfate or nitrate enriched sea-salt or soil particle when excess ammonia gas was available.

[36] In present conditions, formation of the coarse mode ammonium can be attributed to the reaction of $NH_3$ vapor on moist aerosols of soil origin. The stoichiometric ratio of $NH_4^+$ to $SO_4^{2-}$ and $NO_3^-$ are both higher in the fine mode (2.57 and 2.22) and lower in the coarse mode (0.55 and 0.47). This shows that excess ammonia gas is available after the formation of fine mode ammonium laden aerosols. This additional ammonia gas may react with moist aerosols of soil origin to form ammonium sulfate and ammonium nitrate on the coarse mode aerosols. Statistically significant correlation for paired association of the good correlations among sulfate, and nitrate with ammonium in coarse mode (Table 4b) suggests aforementioned possibility.

#### 3.2.5. Sodium

[37] The size distribution curve for water soluble $Na^+$ loading on the aerosol samples collected in shown in Figure 2f. It can be observed that the average water soluble $Na^+$ loading varied in the range 0.04 to 1.02 $\mu g\ m^{-3}$ of aerosol mass collected for various size ranges of the aerosol with higher loading in the very fine (<0.49 $\mu m$) and coarse (3.0–10 $\mu m$) aerosols (refer to Table 3). Much of the water soluble (≈92%) ammonium is obtained from fine mode aerosols.

[38] High loading of $Na^+$ in fine mode aerosols suggests presence of nonmarine other than marine salts. *Parmar et al.* [2001a] have reported highest concentration (about 51%) of $Na^+$ in fine mode during monsoon period at Agra. The source for fine mode $Na^+$ is largely unknown. However, *Hong and Chak* [1997], report that combustion of coal, oil or biomass may be important to the atmospheric loading of fine mode sodium. *Novakov and Corrigan* [1995] also reported emission of sodium from biomass smoke particles. Coarse mode sodium may be mainly soil derived.

#### 3.2.6. Potassium

[39] The size distribution curve for water soluble $K^+$ loading on the aerosol samples collected in shown in Figure 2g. It can be observed that the average water soluble $K^+$ loading varied in the range 0.10 to 2.99 $\mu g\ m^{-3}$ of aerosol mass collected for various size ranges of the aerosol with no significant difference in the fine and coarse aerosols (refer to Table 3). Much of the water soluble (≈ 86%) potassium is obtained from fine mode aerosols.

[40] Predominant fraction in the fine mode indicates the anthropogenic origin of $K^+$. Fine mode $K^+$ is released into the atmosphere through biomass burning [*Cooper and Watson*, 1980; *Penner*, 1995]. However, many other researchers have attributed vegetation as another source of $K^+$ particles [*Kleinman et al.*, 1979]. Plants emit submicron $K^+$ through the respiration mechanism. It is believed that guttation, the process of secretion of water on to the surface of leaves through specialized pores or hydathodes, is the cause of this emission. In this process $K^+$ is transported from roots to leaves and released into the atmosphere through the stomata. This phenomenon takes place during the high humid conditions when the rate of transpiration is low. This condition is generally likely to prevail during the months of December/January (sampling period of the present study) in the region. Refuse burning also contributes to $K^+$ in the fine mode [*Venkataraman et al.*, 2002]. Further nss-$K^+$ contributed to 99% of the total $K^+$. This suggests that the emission of $K^+$ into the atmosphere by biomass burning or vegetation or both. The coarse mode contribution to water soluble potassium could be soil derived, as the other predominant source (i.e., sea salt) is likely to be insignificant.

#### 3.2.7. Calcium and Magnesium

[41] The size distribution curve for water soluble Ca and Mg loading on the aerosol samples collected in shown in Figures 2h and 2i. Unlike other water soluble components referred above, coarse aerosols contribute to the water soluble Ca and Mg to a large extent (refer to Table 3). The total mass of water soluble Ca and Mg in 8 hour $PM_{10}$ samples collected by single-stage sampler is significantly higher (∼50%) than those in 24 hour $PM_{10}$ samples collected by four-stage sampler. This could be due to difference in average wind speeds during the sample collection (9.00–5.00 hours for total $PM_{10}$ mass collection with average wind 3.1 km $h^{-1}$ compared to 24 hour size segregated mass collection with average wind speed 2.3 km $h^{-1}$). The total $PM_{10}$ mass is expected to have much of wind blown dust, and hence more water soluble Ca and Mg.

#### 3.2.8. Charge Balance on Water Soluble Fraction

[42] Cation-to-anion ratio without accounting for $H^+$ and $OH^-$ ions in the water soluble fraction of the $PM_{10}$ mass collected was in the range 1.1–1.8. The pH of the aerosol suspension in distilled, deionized water was roughly around 7. These observations suggest presence of some more anionic species such derived from carbonic and organic acids. These were not analyzed in the water soluble fraction but are likely to be present in biomass and soil derived aerosols.

### 3.3. Part III: Comparative Assessment of Chemical Characteristics of Aerosols During Foggy/Hazy and Clear Days

[43] Results of the partial chemical analysis of aerosols and the synthesis of information related to the plausible chemical reactions in the atmosphere that could be responsible for enhanced aerosol loadings in the region substantiate that significant portions of the aerosols are formed because of emissions from anthropogenic sources such as biomass and fossil fuel burning, excessive use of inorganic fertilizers for enhanced agricultural output, etc. In this part of the study an attempt is made to compare the chemical characteristics of the aerosols on foggy/hazy days with clear days in order to validate the postulation made for the enhanced foggy/hazy conditions in the winter which may enable some control/remedial actions to prevent/reduce foggy/hazy days.

[44] During the entire campaign period, fog episodes occurred in two phases: first phase from 8 to 28 December 2004 except on 26 and 27 December and second phase from

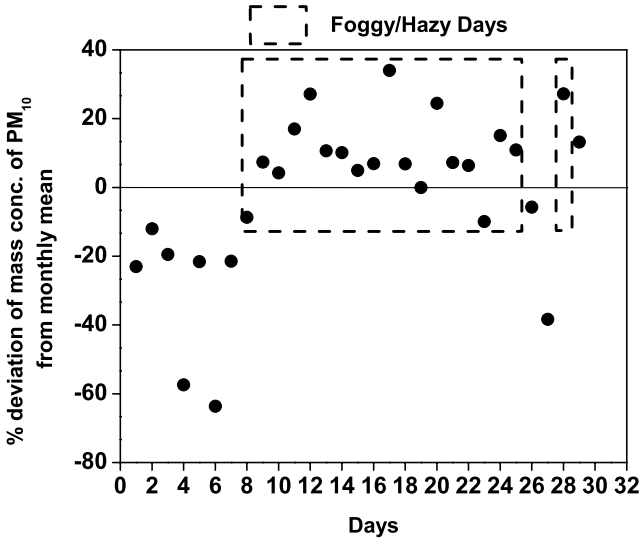


**Figure 4a.** Percentage deviation of the mass concentration of total $PM_{10}$ particulate matter from monthly mean.

2 to 4 January 2005. Generally, formation of fog started in the early evening and it persisted till the late morning next day. A light rain of short duration had occurred during night on 2 January 2005.

### 3.3.1. $PM_{10}$ Mass Loading

[45] Deviation in mass of $PM_{10}$ aerosols collected on every day from monthly mean is shown in Figure 4a (shaded portions indicate foggy/hazy periods). Trends indicate positive deviations from monthly mean during the foggy/hazy periods because of increase in particulate mass concentration on those days. This is due to the substantial increment of accumulation mode particle concentration (which is incorporated within fine mode) just preceding the foggy/hazy conditions or during the occurrence of fog/haze episodes. Accumulation mode particles generally act as condensation nuclei, which form fog droplets upon condensation of water vapor [*Seinfeld and Pandis*, 1998]. This increment is also confirmed from the results obtained by quartz crystal microbalance (QCM) data during the same period [see *Tripathi et al.*, 2006].

### 3.3.2. Water Soluble Ions

[46] The average percentage contributions of all water soluble ions and acid soluble metals in $PM_{10}$ mass collected during foggy/hazy and clear days are shown in Figure 4b. Error bars indicate the standard deviation in the magnitude of each species from the mean values during both foggy/hazy and clear days. $NO_3^-$ and $NH_4^+$ ions showed considerable increase in their percentage contribution during foggy/hazy day compared to the clear days. A reverse trend is observed for water soluble Ca and Mg, and acid soluble metals (Al, Fe and Ca). Figure 5 presents the percentage deviation of ratio of $SO_4^{2-}$, $NO_3^-$ and $NH_4^+$ concentration to $PM_{10}$ concentration from monthly mean on every sampling day. Ammonium and nitrates are generally higher during foggy/hazy period. Ammonium often accompanies sulfate formed as the neutralizing cation [*Seinfeld and Pandis*, 1998] where presence of higher concentration of $NH_3$ gas and $HNO_3$ favor the formation of particulate ammonium nitrate at suitable relative humidity and temperature through various reactions explained in the previous section.

### 3.3.3. Black Carbon

[47] BC concentration varied in the range 6–20.1 $\mu g\ m^{-3}$ diurnally [*Tripathi et al.*, 2005a]. Deviation in mass concentration of BC on every day from monthly mean is shown in Figure 6 (shaded portions indicate foggy/hazy periods). Higher mass concentrations of BC were observed during foggy/hazy periods.

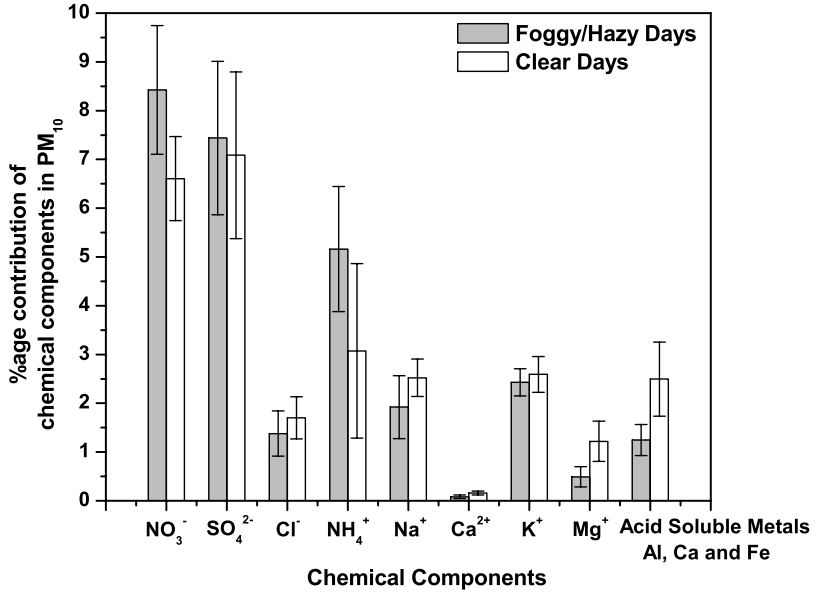


**Figure 4b.** Percentage contribution of each chemical component in total $PM_{10}$ particulate matter during foggy/hazy and clear days (standard deviations shown as error bars).

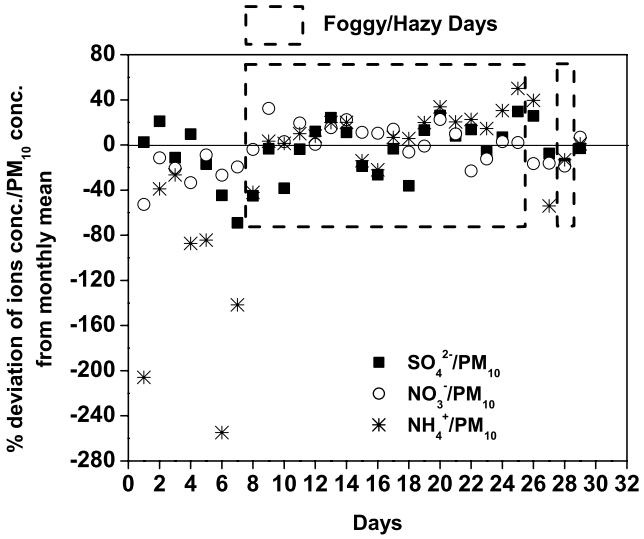


**Figure 5.** Percentage deviation of ratio of ion concentration to $PM_{10}$ mass concentration from monthly mean.

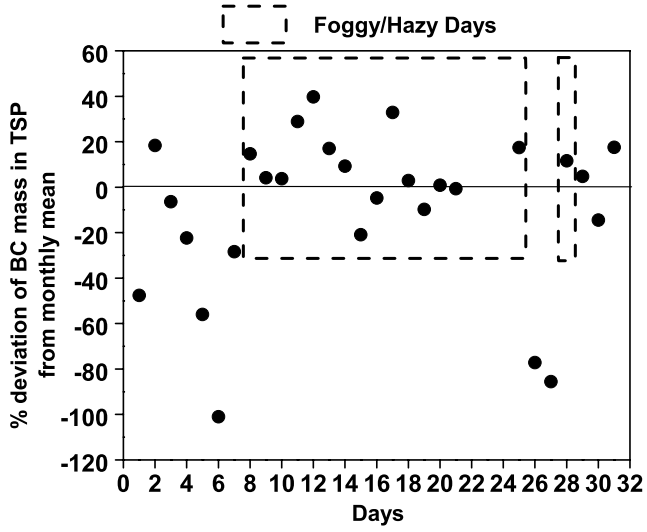


**Figure 6.** Percentage deviation of BC mass concentration in total suspended matter from the monthly mean.

### 3.3.4. Statistical Analysis

[48] Table 6 presents the results of the statistical analysis carried out to compare the various aerosol parameters between foggy/hazy and clear days. The analysis is done on the basis of difference in mean values at 5% significance level. The results indicate that aerosol loadings, water soluble $NO_3^-$ and $NH_4^+$ of aerosols (likely to be originated from gaseous anthropogenic emissions in the region), and BC are significantly higher during the foggy/hazy days as compared to clear days and may be responsible for enhanced and prolonged foggy/hazy conditions. The other water soluble species such as $SO_4^-$, $Cl^-$, $K^+$, and $Na^+$ are also likely to be originated from regional anthropogenic emissions but there levels are not found to be significantly different in foggy/hazy and clear days. The water soluble $Ca^{2+}$ and $Mg^{2+}$, which are essentially soil derived and mostly in coarse aerosols, are significantly lower during foggy/hazy days compared to clear days.

## 4. Conclusions

[49] Partial chemical analysis of total and size segregated aerosols collected daily at a typical location in the Ganga basin in Northern India measured during a comprehensive field campaign in the winter season (December 2004) are presented. The major conclusions may be stated as follows.

[50] 1. The $PM_{10}$ and black carbon (BC) mass concentrations are significantly higher during the foggy/hazy period. Much of the $PM_{10}$ mass ($\approx$ 81%) is due to fine/accumulation mode particles (0.1–0.95 $\mu$m).

[51] 2. Significant proportions of water soluble ions such as $NH_4^+$, $K^+$, $Na^+$, $Cl^-$, $NO_3^-$ and $SO_4^{2-}$ are present in the fine mode particles while considerable amounts of $Ca^{2+}$ and $Mg^{2+}$ along with $NH_4^+$, $K^+$, $Na^+$, $Cl^-$, $NO_3^-$ and $SO_4^{2-}$ are present in the coarse mode particles.

[52] 3. Water soluble ions $NH_4^+$ and $NO_3^-$ are significantly higher while $Ca^{2+}$, $Mg^{2+}$ and acid soluble metals are significantly lower in the aerosols collected during foggy/hazy days as compared to the clear days.

[53] 4. Presence of higher amounts of $NH_4^+$, $K^+$, $NO_3^-$ and $SO_4^{2-}$ associated with very low values (<5 ppmv) of $SO_2$ despite considerable plausible emissions due to fossil fuel and biomass burning in the region suggests that loading of fine mode aerosols in the region could have been enhanced through reactions of gaseous pollutants on the solid surfaces.

[54] 5. Aerosol loadings, water soluble $NO_3^-$ and $NH_4^+$ of aerosols (likely to be originated from gaseous anthropogenic emissions in the region), and BC are significantly higher during the foggy/hazy days as compared to clear days and may be responsible for enhanced and prolonged foggy/hazy conditions.

[55] 6. The other water soluble species such as $SO_4^-$, $Cl^-$, $K^+$, and $Na^+$ are also likely to be originated from regional

**Table 6.** Significance of Particulate Matter and Various Chemical Components During Foggy/Hazy and Clear Days

| Component | Concentration in Foggy/Hazy Days, $\mu g\ m^{-3}$ | Concentration in Clear Days, $\mu g\ m^{-3}$ | Statistical Inference at 5% Significance[a] |
|---|---|---|---|
| $PM_{10}$ | 231.6 ± 43.3 | 175.1 ± 33.1 | F/N ↑ |
| $NO_3^-$ | 19.6 ± 5.3 | 11.8 ± 3.7 | F/N ↑ |
| $SO_4^{2-}$ | 17.2 ± 4.9 | 12.6 ± 4.4 | F/N ↔ |
| $Cl^-$ | 3.1 ± 1.0 | 3.0 ± 1.0 | F/N ↔ |
| $NH_4^+$ | 11.8 ± 3.0 | 5.7 ± 4.1 | F/N ↑ |
| $Na^+$ | 4.3 ± 0.9 | 4.4 ± 1.0 | F/N ↔ |
| $K^+$ | 5.6 ± 0.8 | 4.5 ± 1.0 | F/N ↔ |
| $Ca^{2+}$ | 1.2 ± 0.5 | 2.1 ± 0.7 | F/N ↓ |
| $Mg^{2+}$ | 0.2 ± 0.8 | 0.3 ± 0.1 | F/N ↓ |
| Al | 0.8 ± 0.5 | 1.4 ± 0.8 | F/N ↓ |
| Fe | 1.7 ± 0.4 | 2.6 ± 0.6 | F/N ↓ |
| Ca | 1.4 ± 0.5 | 2.4 ± 0.8 | F/N ↓ |
| BC | 14.3 ± 2.7 | 9.8 ± 3.0 | F/N ↑ |

[a]F/N ↑ indicates that foggy/hazy period level is significantly high; F/N ↓ indicates that clear period level is significantly high; F/N ↔ indicates no significant difference.

anthropogenic emissions but there levels are not found to be significantly different in foggy/hazy and clear days.

[56] **Acknowledgments.** This work is carried out under Indian Space Research Organization's Geosphere Biosphere Program Land Campaign II. S.N.T. acknowledges helpful discussion with Chandra Venkataraman.

## References


Alfaro, S. C., A. Gaudichet, J. L. Rajot, L. Gomes, M. Maillé, and H. Cachier (2003), Variability of aerosol size-resolved composition at an Indian coastal site during the Indian Ocean Experiment (INDOEX) intensive field phase, *J. Geophys. Res.*, *108*(D8), 4235, doi:10.1029/2002JD002645.

Andreae, M. O., and P. Merlet (2001), Emission of trace gases and aerosolsfrom biomass burning, *Global Biogeochem. Cycles*, *15*, 955–966.

Andreae, M., et al. (1988), Biomass-burning emissions and associated haze layers over Amazonia, *J. Geophys. Res.*, *93*, 1509–1527.

Charlson, R. J., S. E. Schwartz, J. M. Hales, R. D. Cess, J. A. Coakley, J. E. Hansen, and D. J. Hofmann (1992), Climate forcing by anthropogenic aerosol, *Science*, *255*, 423–430.

Cheng, Z. L., K. S. Lam, L. Y. Chan, T. Wang, and K. K. Cheng (2000), Chemical characteristics of aerosols at coastal station in Hong Kong. Seasonal variation of major ions, halogens and mineral dusts between 1995 and 1996, *Atmos. Environ.*, *34*, 2771–2783.

Chu, D. A., Y. J. Kaufman, G. Zibordi, J. D. Chern, J. Mao, C. Li, and B. N. Holben (2003), Global monitoring of air pollution over land from the Earth Observing System-Terra Moderate Resolution Imaging Spectroradiometer (MODIS), *J. Geophys. Res.*, *108*(D21), 4661, doi:10.1029/2002JD003179.

Cooper, J. A., and J. G. Watson (1980), Receptor oriented methods of air particulate source apportionment, *J. Air Pollut. Control Assoc.*, *30*(10), 1116–1125.

Corbin, K. C., S. M. Kreidenweis, and T. H. Vonder Haar (2002), Comparison of aerosol properties derived from Sun photometer data and ground-based chemical measurements, *Geophys. Res. Lett.*, *29*(10), 1363, doi:10.1029/2001GL014105.

Dey, S., S. N. Tripathi, R. P. Singh, and B. N. Holben (2006), Retrieval of black carbon and specific absorption over Kanpur city, Northern India during 2001–2003 using AERONET data, *Atmos. Environ.*, *40*, 445–456.

Dickerson, R. R., S. Kondragunta, G. Stenchikov, K. L. Civerolo, B. G. Doddrige, and B. N. Holben (1997), The impact of aerosols on solar ultraviolet radiation and photochemical smog, *Science*, *278*, 827–830.

Finlayson-Pitts, B. J., and J. N. Pitts Jr. (2000), *Chemistry of the Upper and Lower Atmosphere*, Elsevier, New York.

Gabriel, R., O. L. Mayol-Bracero, and M. O. Andreae (2002), Chemical characterization of submicron aerosol particles collected over the Indian Ocean, *J. Geophys. Res.*, *107*(D19), 8005, doi:10.1029/2000JD000034.

Girolamo, L. D., et al. (2004), Analysis of Multi-angle Imaging SpectroRadiometer (MISR) aerosol optical depths over greater India during winter 2001–2004, *Geophys. Res. Lett.*, *31*, L23115, doi:10.1029/2004GL021273.

Gonzalez, G. R., M. Schaap, G. De Leeuw, P. J. H. Builtjes, and M. Van Loon (2003), Spatial variations of aerosol properties over Europe derived from satellite observations and comparison with model calculations, *Atmos. Chem. Phys.*, *3*, 521–533.

Harman, H. H. (1960), *Modern Factor Analysis*, Univ. of Chicago Press, Chicago, III.

Haywood, J. M., and V. Ramaswamy (1998), Global sensitivity studies of the direct radiative forcing due to anthropogenic sulfate and black carbon aerosols, *J. Geophys. Res.*, *103*, 6043–6058.

Hering, S. V., and S. K. Friedlander (1982), Origins of aerosol sulphur size distributions in the Los Angels basin, *Atmos. Environ.*, *16*, 2647–2656.

Hillamo, R. E., and E. I. Kauppinen (1991), Size distributions of inorganic ions in atmospheric aerosol in Norway, *Aerosol Sci. Technol.*, *14*, 33–47.

Hitchcock, D. R., L. L. Spiller, and W. E. Wilson (1980), Sulfuric acid aerosols and HCl release in coastal atmospheres: Evidence of rapid formation of sulphuric acid particulates, *Atmos. Environ.*, *14*, 165–182.

Hobbs, P. V., J. S. Reid, R. A. Kotchenruther, R. J. Ferek, and R. Weiss (1997), Direct radiative forcing by smoke from biomass burning, *Science*, *275*, 1776–1778.

Hong, Z., and K. C. Chak (1997), Size distribution of inorganic aerosols at a coastal site, *J. Aerosol Sci.*, *28*(101), 213–214.

Kaneyasu, N., H. Yoshikado, M. Hiroshi, T. Mizuno, K. Sakamoto, and M. Soufuku (1999), Chemical forms and sources of extremely high nitrate and chloride in winter aerosol pollution in the Kanto Plain of Japan, *Atmos. Environ.*, *33*(11), 1745–1756.

Kapoor, R. K., G. Singh, and S. Tiwari (1992), Ammonia concentration vis-à-vis meteorological conditions at Delhi, India, *Atmos. Res.*, *28*, 1–9.

Kaufman, Y. J., D. Tanre, H. R. Gordan, T. Nakajima, J. Lenoble, R. Frouin, H. Grassl, B. M. Herman, M. D. King, and P. M. Teillet (1997), Passive remote sensing of tropospheric aerosol and atmospheric correction for aerosol characterization, *Remote Sens. Environ.*, *66*, 1–16.

Kermein, V. M., and A. S. Wexler (1995), Growth laws for atmospheric aerosol particles: An examination of the bimodality of the accumulation mode, *Atmos. Environ.*, *29*, 3263–3275.

Kishore, S. (2005), Investigation into seasonal and diurnal formation of atmospheric nitrate, M.Tech. thesis, Indian Inst. of Technol., Kanpur, India.

Kleinman, M. T., C. Tomezyk, B. P. Leaderer, and R. L. Tanner (1979), Inorganic nitrogen compounds in New York City, *Air Annu. N. Y. Acad. Sci.*, *322*, 115–123.

Kulshrestha, U., A. Saxena, N. Kumar, K. M. Kumari, and S. S. Srivastava (1998), Chemical composition and association of size-differentiated aerosols at a suburban site in a semi-arid tract of India, *J. Aerosol Chem.*, *29*(20), 109–118.

Lazaridis, M., A. Semb, and Ø. Hov (1999), Long-range transport of aerosol particles—A literature review, *EMEP/CCC Rep. 8/99*, Norw. Inst. of Air Res., Kjeller, Norway.

Lelieveld, J., et al. (2001), The Indian Ocean Experiment: Widespread air pollution from South and Southeast Asia, *Science*, *291*, 1031–1036.

Lewandowska, A., F. Lucyna, and B. Magdalena (2004), Ammonia and ammonium over the southern Baltic Sea, part 2. The origin of ammonia and ammonium over two stations: Gdynia and Hel, *Oceanologia*, *46*(2), 185–200.

Ma, J., J. Tang, S.-M. Li, and M. Z. Jacobson (2003), Size distribution of ionic aerosols measured at Waliguan Observatory: Implication for nitrate gas-to-particle transfer processes in the free troposphere, *J. Geophys. Res.*, *108*(D17), 4541, doi:10.1029/2002JD003356.

Ma, Y., et al. (2003), Characteristics and influence of biosmoke on the fine-particle ionic composition measured in Asian outflow during the Transport and Chemical Evolution Over the Pacific (TRACE-P) experiment, *J. Geophys. Res.*, *108*(D21), 8816, doi:10.1029/2002JD003128.

Meng, Z., and J. H. Seinfeld (1994), On the source of the submicrometer droplet mode of urban and regional aerosols, *Aerosol Sci. Technol.*, *20*, 253–265.

Millero, F. J., and M. L. Sohn (1992), *Chemical Oceanography*, 531 pp., CRC Press, Boca Raton, Fla.

Moorthy, K. K., et al. (2005), Wintertime spatial characteristics of boundary layer aerosols over peninsular India, *J. Geophys. Res.*, *110*, D08207, doi:10.1029/2004JD005520.

Nadstazik, A., R. Marks, and M. Schulz (2000), Nitrogen species and macro elements in aerosols over the southern Baltic Sea, *Oceanologia*, *42*(4), 411–424.

Novakov, T., and C. E. Corrigan (1995), Thermal characterization of biomass smoke particles, *Mikrochim. Acta*, *119*, 157–166.

Pandis, S. N., and J. H. Seinfeld (1989), Mathematical modeling of acid deposition due to radiation fog, *J. Geophys. Res.*, *94*(D10), 12,911–12,923.

Pandis, S. N., J. H. Seinfeld, and C. Pilnis (1992), Heterogeneous sulfate production in an urban fog, *Atmos. Environ.*, *26*, 2509–2522.

Parmar, R. S., G. S. Satsangi, M. Kumari, A. Lakhani, S. S. Srivastava, and S. Prakash (2001a), Study of size distribution of atmospheric aerosol at Agra, *Atmos. Environ.*, *35*, 693–702.

Parmar, R. S., G. S. Satsangi, M. Kumari, A. Lakhani, S. S. Srivastava, and S. Prakash (2001b), Simultaneous measurements of ammonia and nitric acid in ambient air at Agra (27°10′N and 78°05′E) (India), *Atmos. Environ.*, *35*, 5979–5988.

Penner, J. E. (1995), Carbonaceous aerosols influencing atmospheric radiation: Black carbon and organic carbon, in *Aerosol Forcing of Climate*, edited by R. J. Charlson and J. Heintzenberg, pp. 91–108, John Wiley, Hoboken, N. J.

Pio, C. A., and R. W. Harrison (1987), Vapor pressure of ammonium chloride aerosol: Effect of temperature and humidity, *Atmos. Environ.*, *21*, 2711–2715.

Ramanathan, V., and M. V. Ramana (2005), Persistent, widespread, and strongly absorbing haze over the Himalayan foothills and the Indo-Gangetic plains, *Pure Appl. Geophys.*, *162*, 1609–1626.

Ramanathan, V., et al. (2001), Indian Ocean Experiment: An integrated analysis of the climate forcing and effects of the great Indo-Asian haze, *J. Geophys. Res.*, *106*, 28,371–28,398.

Rencher, A. C. (2002), Factor analysis, in *Methods of Multivariate Analysis*, 2nd ed., pp. 408–450, John Wiley, Hoboken, N. J.

Satheesh, S. K., V. Ramanathan, X. Li-Jones, J. M. Lobert, I. A. Podgorny, J. M. Prospero, B. N. Holben, and N. G. Loeb (1999), A model for the natural and anthropogenic aerosols over the tropical Indian Ocean derived from Indian Ocean Experiment data, *J. Geophys. Res.*, *104*(D22), 27,421–27,440.

Satheesh, S. K., V. Ramanathan, B. N. Holben, K. K. Moorthy, N. G. Loeb, H. Maring, J. M. Prospero, and D. Savoie (2002), Chemical, microphysical and radiative effects of Indian Ocean aerosols, *J. Geophys. Res.*, *107*(D23), 4725, doi:10.1029/2002JD002463.

Satoshi, K. (1976), Size distribution of atmospheric total aerosols, sulfate, ammonium and nitrate particulates in the Nagoya area, *Atmos. Environ.*, *10*, 39–43.

Savoie, D. L., and J. M. Prospero (1982), Particle size distribution of nitrate and sulfate in the marine atmosphere, *Geophys. Res. Lett.*, *9*, 1207–1210.

Saxena, P., and C. Seigneur (1987), On the oxidation of $SO_2$ to sulfate in atmospheric aerosols, *Atmos. Environ.*, *21*, 807–812.

Seinfeld, J. H., and S. N. Pandis (1998), *Atmospheric Chemistry and Physics*, Wiley-Intersicence, Hoboken, N. J.

Sharma, M., Y. N. V. M. Kiran, and K. K. Shandilya (2003), Investigations into formation of atmospheric sulfate under high $PM_{10}$ concentration, *Atmos. Environ.*, *37*, 2005–2013.

Sudesh, Y., and V. Rajamani (2004), Geochemistry of aerosols of northwestern part of India adjoining the Thar Desert, *Geochim. Cosmochim. Acta*, *68*(9), 1975–1988, doi:10.1016/j.gca.2003.10.032.

Tabazadeh, A., M. Z. Jacobson, H. B. Singh, O. B. Toon, J. S. Lin, R. B. Chatfield, A. N. Thakur, R. W. Talbot, and J. E. Dibb (1998), Nitric acid scavenging by mineral and biomass aerosols, *Geophys. Res. Lett.*, *25*, 4185–4188.

Talbot, R. W., M. O. Andreae, T. W. Andreae, and R. C. Harriss (1988), Regional aerosol chemistry of the Amazon basin during the dry season, *J. Geophys. Res.*, *93*, 1499–1508.

Tripathi, S. N., S. Dey, V. Tare, and S. K. Satheesh (2005a), Aerosol black carbon radiative forcing at an industrial city in northern India, *Geophys. Res. Lett.*, *32*, L08802, doi:10.1029/2005GL022515.

Tripathi, S. N., S. Dey, V. Tare, S. K. Satheesh, S. Lal, and S. Venkataramni (2005b), Enhanced layer of black carbon in north Indian industrial city, *Geophys. Res. Lett.*, *32*, L12802, doi:10.1029/2005GL022564.

Tripathi, S. N., et al. (2006), Measurements of atmospheric parameters during ISRO-GBP Land Campaign II at a typical location in Ganga Basin: 1. Physical and optical properties, *J. Geophys. Res.*, *111*, D23209, doi:10.1029/2006JD007278.

Uehara, G. (2005), Volcanic soils, in *Encyclopedia of Soils in the Environment*, vol. 4, edited by D. Hillel, pp. 225–232, Elsevier, New York.

U.S. Environmental Protection Agency (1999), Compendium methods IO-3.1 and 3.2, Washington, D. C.

Venkataraman, C., P. Sinha, and B. Sachin (2001), Sulfate aerosol distribution at Mumbai, India during the INDEOX-IFP (1998), *Atmos. Environ.*, *35*, 2647–2655.

Venkataraman, C., C. K. Reddy, S. Josson, and M. S. Reddy (2002), Aerosol size and chemical characteristics at Mumbai, India, during the INDOEX-IFP (1999), *Atmos. Environ.*, *36*, 1979–1991.

Venkataraman, C., G. Habib, D. Kadamba, M. Shrivastava, J.-F. Leon, B. Crouzille, O. Boucher, and D. G. Streets (2006), Emissions from open biomass burning in India: integrating the inventory approach with high-resolution Moderate Resolution Imaging Spectroradiometer (MODIS) active fire and land count data, *Global Biogeochem. Cycles*, *20*, GB2013, doi:10.1029/2005GB002547.

Wall, S. M., W. John, and J. L. Ondo (1988), Measurement of aerosol size distributions for nitrate and major ionic species, *Atmos. Environ.*, *22*, 1649–1656.

Willison, M. J., A. G. Clarke, and E. M. Zeki (1989), Chloride aerosols in central northern England, *Atmos. Environ.*, *23*(10), 2231–2239.

Zhuang, H., K. Chak, M. F. Chan, and A. S. Wexler (1999), Size distribution of particulate sulfate, nitrate and ammonium at a coastal site in Hong Kong, *Atmos. Environ.*, *33*, 843–853.

A. Agarwal, N. Chinnam, S. Dey, V. P. Kanawade, S. Kishore, R. B. Lal, M. Manar, M. Sharma, A. K. Srivastava, V. Tare, and S. N. Tripathi, Department of Civil Engineering, Indian Institute of Technology, Kanpur 208016, India. (snt@iitk.ac.in)